

---

This is an electronic reprint of the original article.  
This reprint may differ from the original in pagination and typographic detail.

Kärhä, Petri; Baumgartner, Hans; Askola, Janne; Kylmänen, Kasperi; Oksanen, Benjamin; Maham, Kinza; Huynh, Vo; Ikonen, Erkki

## Measurement setup for differential spectral responsivity of solar cells

*Published in:*  
Optical Review

*DOI:*  
[10.1007/s10043-020-00584-x](https://doi.org/10.1007/s10043-020-00584-x)

Published: 01/04/2020

*Document Version*  
Publisher's PDF, also known as Version of record

*Published under the following license:*  
CC BY

*Please cite the original version:*  
Kärhä, P., Baumgartner, H., Askola, J., Kylmänen, K., Oksanen, B., Maham, K., Huynh, V., & Ikonen, E. (2020). Measurement setup for differential spectral responsivity of solar cells. *Optical Review*, 27(2), 195 - 204. <https://doi.org/10.1007/s10043-020-00584-x>



The 13th Japan-Finland Joint Symposium on Optics in Engineering (OIE'19), Espoo, Finland and Tallinn, Estonia

# Measurement setup for differential spectral responsivity of solar cells

Petri Kärhä<sup>1</sup> · Hans Baumgartner<sup>1</sup> · Janne Askola<sup>1</sup> · Kasperi Kylmänen<sup>1</sup> · Benjamin Oksanen<sup>1</sup> · Kinza Maham<sup>1</sup> · Vo Huynh<sup>1</sup> · Erkki Ikonen<sup>1,2</sup>

Received: 15 October 2019 / Accepted: 27 January 2020  
© The Author(s) 2020

## Abstract

We have developed a setup for measuring differential spectral responsivities of unifacial and bifacial solar cells under bias light conditions. The setup uses 30 high-brightness LEDs for generating a quasi-monochromatic light source covering the wavelength range 290–1300 nm. Halogen lamps are used to generate bias-lighting conditions up to the irradiance level of 1000 W/m<sup>2</sup>. The setup has been fully characterized for spectral irradiances and spatial uniformities of all light sources. Validation measurements carried out using a reference cell of 2 × 2 cm<sup>2</sup> area from Fraunhofer ISE demonstrated an agreement better than 2% over the wavelength range of 425–940 nm, with an expanded uncertainty of 2.6%. In the UV and IR regions, the discrepancies are higher but still within estimated uncertainties. The setup is also tested in measuring spectral responsivities of large 15 × 15 cm<sup>2</sup> bifacial solar cells. The associated problems are discussed.

**Keywords** Radiometry · Solar cell · Spectral responsivity · Efficacy · Electricity · Bifacial

## 1 Introduction

Spectral responsivity of a photovoltaic device is needed for solar cell development and cell analysis. It can also be used in testing of solar cells, to correct for the spectral mismatch between the light source used in the measurement from the standardized reference spectral irradiance data. Measurement setups of spectral responsivity have been standardized in [1]. Solar cells can be nonlinear which poses a challenge in measurements. The solar cells need to be measured in biased conditions, resulting in differential spectral responsivity. Standard Test Conditions (STC) for measuring the performance of PV modules specify a cell temperature of 25 °C and an irradiance of 1000 W/m<sup>2</sup> with an air mass 1.5 (AM1.5) spectrum [2]. This standardized spectrum is called AM1.5G (global) in earlier standards. Tests can also be carried out at other irradiance levels within 5–110% of the standard test condition.

Measurement setups for differential spectral responsivity have been presented in e.g. [3–7]. The cells measured are biased with incandescent or Xe light sources. Monochromatic measurement beam is chopped and measured with a lock-in amplifier from the cell output. The monochromatic beam is typically realized with a monochromator or filters and a broadband source. Combining the bias light with the measurement beam can be made in an integrating sphere, or the beams can be imposed on the cell surface. Recently, also setups where lighting is provided by LEDs have been presented [8–10]. LED lighting has been demonstrated both for use as bias lighting with accurately set spectrum and for probe lighting using electrical modulation and a lock-in amplifier.

In this paper, we present a measurement setup for differential spectral responsivity of solar cells based on high-power LEDs used as quasi-monochromatic sources of light for spectral measurement. LEDs offer advantages over monochromators, including more compact size, higher intensity, stability, and simpler modulation using electronics. On the other hand, they have broader bandwidths, which complicates the data analysis.

The solar cells to be measured are biased with halogen lamps up to a lighting level of 1000 W/m<sup>2</sup>. Additional

✉ Petri Kärhä  
petri.karha@aalto.fi

<sup>1</sup> Metrology Research Institute, Aalto University, Espoo, Finland

<sup>2</sup> VTT MIKES, Espoo, Finland

halogen lamps have been installed behind the cell to measure bifacial solar cells with both sides biased.

The measurement setup is presented in details in Sect. 2. The properties of the setup have been thoroughly characterized. The results of the characterizations are presented in Sect. 3. The methods for data analysis are described in Sect. 4. To validate the setup, comparison measurements have been carried out by measuring a  $2 \times 2 \text{ cm}^2$  reference solar cell provided by Fraunhofer Institute for Solar Energy (ISE). The absolute differential spectral responsivity of the cell has been measured at  $25^\circ\text{C}$  in a wavelength range from 300 to 1200 nm at a short-circuit current bias, which assures that the calibrated values are equal to the absolute spectral response at Standard Testing Conditions (STC). The results of the validation measurements are reported in Sect. 5 and compared to obtained measurement uncertainties. We also demonstrate use of the setup for measuring a bifacial solar cell with relatively large size of  $15 \times 15 \text{ cm}^2$ . Finally, conclusions are drawn in Sect. 6.

## 2 Equipment

The measurement setup for differential spectral responsivity of solar cells is presented in Fig. 1. The setup utilizes towers of halogen lights, each tower containing 7 pieces of 50 W

lamps for bias light, and 30 narrow-band LEDs for measurement. There are four towers for lighting the front surface of the cell. In addition, two towers have been installed behind the cell for measuring bifacial cells [11]. The lamps installed are of type OSRAM Decostar 50 W. These lamps have a semitransparent aluminum back reflector that modifies the spectrum in the infrared region, and a UV block. Intensity levels in our setup are adjusted by changing the distance between the lamps and the sample, by switching of complete light towers or lamps within them, and by adjusting the current.

The measurement LEDs are mounted in a carousel, guiding one LED at a time to light the cell. The carousel has been earlier used in measurement of cameras [12]. The LEDs are temperature controlled to  $25^\circ\text{C}$  and driven with a modulated operating current. A lock-in amplifier Stanford Research Systems SR830 is used to detect the weak LED signal from the induced photocurrent of the solar cell.

The reference solar cell measured has a built-in temperature sensor. For simple unifacial cells, we have a temperature controller that can be used to set the temperature of the cell to  $25^\circ\text{C}$ . This special temperature controller [13] combines liquid cooling and electrical heating. The bifacial solar cells measured cannot be controlled for temperature.

The photocurrent of the solar cell is measured with a shunt resistor ( $2 \Omega$ ) that converts the photocurrent to voltage

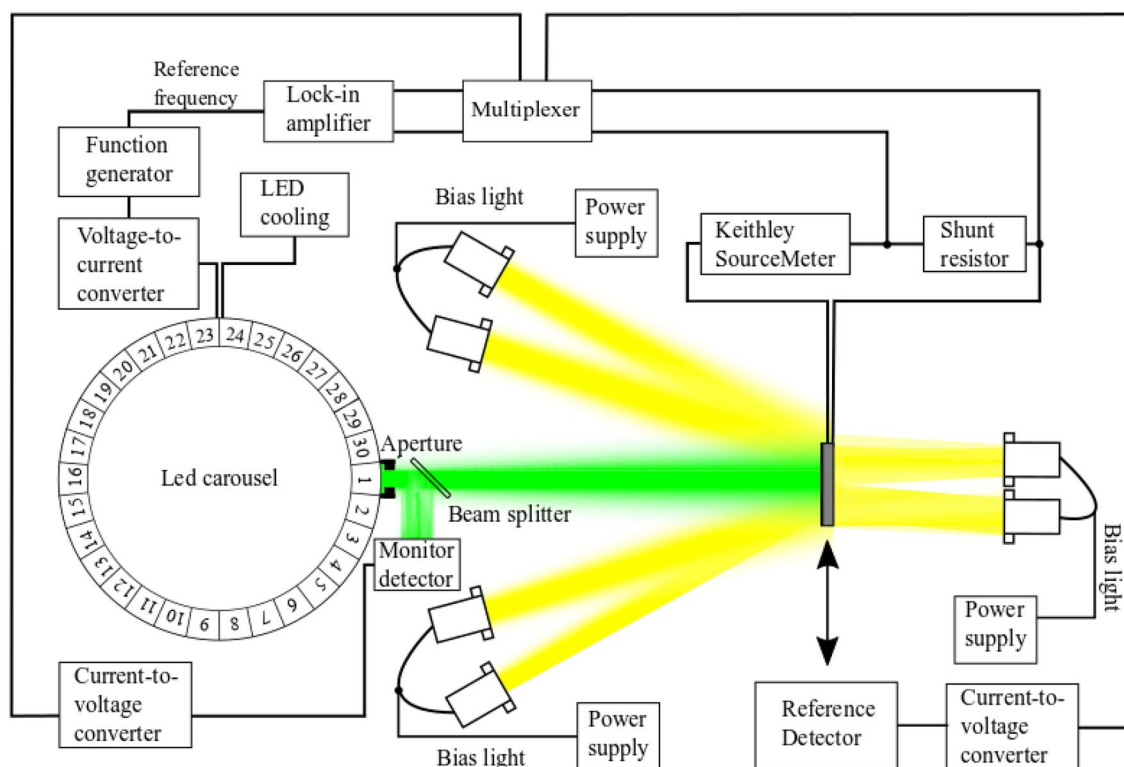


**Fig. 1** Schematic presentation of the differential spectral responsivity setup configured for measurement of a bifacial cell

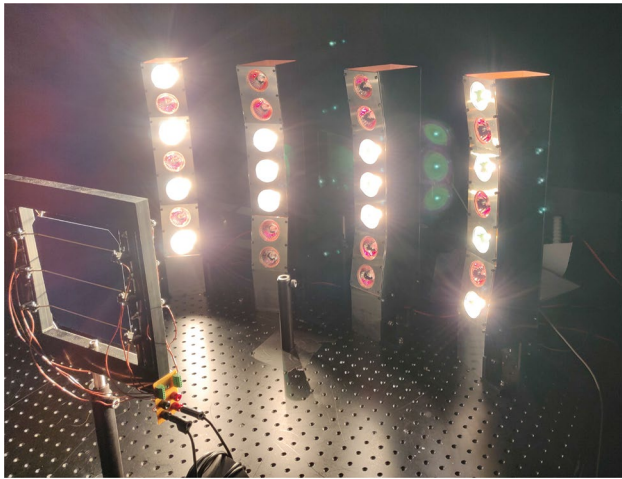


**Fig. 2** Four towers containing the front bias lights, 7 pieces of 50 W halogen lamps in each tower. In the figure, half the lights are lit providing approximately  $500 \text{ W/m}^2$  on the surface of the solar cell on the left. Two additional towers can be used when measuring bifacial solar cells for providing light for the rear side of the cells

for the lock-in-amplifier. A Keithley 2420 source meter is used to keep the voltage across the cell negligible. The current range of the source meter is limited to 3 A, which prevented its use in measuring the large bifacial cell that produces currents above 6 A. For the large solar cell, a zero-flux current sensor from Danisense (DS200ID-CD1000 sensor with DSSIU-6-1U electronics) was used to measure the current. The cell was short circuited with a 1-m cable that was passed through the sensor 8 times. The sensor attenuates the signal with a factor of 500 resulting overall to attenuation of  $500/8$  in the signal level.

Current to the LEDs is provided by a function generator Agilent 33521A and a custom-made voltage-to-current converter that provides a current of 100 mA for each 1 V in the input. In differential responsivity measurements, the LEDs are modulated with a square wave at a frequency of 177 Hz. The pulsed current is biased to vary between 0 and 200 mA. In spectral irradiance and spatial uniformity measurements, the LEDs are driven with a constant DC current of 200 mA. Electronics connect the current to one LED at a time. The electronics also connect the temperature controller electronics to the LED being used.

The bias light towers (Fig. 2) are driven with 1 kW Heininger PTN 125-10 power supplies, each supplying current for two towers. The halogen lamps in towers are connected in series and the two towers are connected in parallel. The front towers are supplied with a current of 7.6 A. Rear towers are tuned in measurements with current and geometry to give one-third of the current that the front lights induce.

LEDs are mounted in black aluminum blocks as can be seen in Fig. 3. The blocks contain temperature sensors providing feedback to the temperature controller electronics.

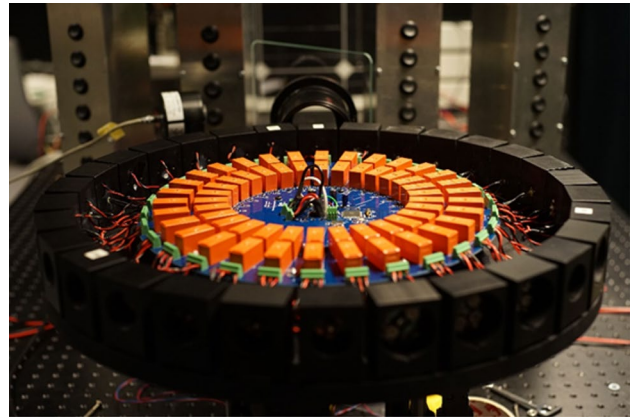


**Fig. 3** A carousel containing the LEDs. The round circuit board in the middle contains relays used for connecting the electronics to one LED at a time. The electronics include a precision current source, a temperature sensor mounted near the LED and temperature controller electronics providing current to thermoelectric elements assembled between the bottom plate and the blocks containing LEDs. The figure also shows a beam splitter and a monitor detector used for accounting beam instabilities, and the back sides of the front bias light towers with switches for the individual lamps

Under the blocks, there are thermoelectric Peltier elements that transfer heat from the LED being used to the bottom plate of the carousel, thus stabilizing the LED temperature to  $25^\circ\text{C}$ . The actual temperature of the LED may be higher than this due to the heating of the LED itself, but the temperature is repeatable provided that the environmental temperature and the operating current are kept constant.

The spectral irradiance on the sample plane is measured with a reference detector consisting of a calibrated silicon trap detector with known spectral responsivity within 250–1300 nm, and a precision aperture with a diameter of 3 mm [14]. In addition, relative spectral irradiances at the sample plane have been measured. The responsivity of the trap detector is accurately known up to 940 nm. Beyond this, the detector responsivity was extrapolated and verified with measurements against a pyroelectric radiometer and a calibrated InGaAs photodiode. The silicon detector has significant responsivity up to 1300 nm, but the uncertainty is much higher than in the visible due to lower signal levels and temperature effects. The irradiance measured can be converted to optical power by multiplying with the detector or solar cell area and vice versa. In addition, a correction is used for the spatial uniformity of the beam.

Short-term drift of the LED intensities can be corrected using a beam splitter and a monitor detector. As a monitor detector, a silicon trap detector is used. For monitoring purposes, a silicon detector works satisfactorily also with the IR LEDs. The monitor was not used in all measurements, because the beam splitter attenuates the signal, which causes problems with low intensity levels in the UV and IR regions.



The LEDs are stable enough to maintain their spectral irradiance for periods of several days without introducing significant uncertainty.

The signals from the current-to-voltage converters used with the trap detectors, and the voltage across the resistor used to convert the cell current to voltage are connected to the lock-in amplifier with a multiplexer. The voltage across the resistor is measured differentially, thus the signal is read by two cables. The other signals are unipolar.

The setup has been tested on a  $2 \times 2 \text{ cm}^2$  reference cell,  $15 \times 15 \text{ cm}^2$  unifacial cells, and  $15 \times 15 \text{ cm}^2$  bifacial cells. Larger cells are supported with a special holder presented in Fig. 4. There are six brass contacts on springs collecting the current from the busbars on the cells. For measuring bifacial solar cells, there are additional six contacts on the rear side of the holder.

### 3 Characterization measurements

The setup has been fully characterized and tested for measurements. The radiation field at the sample plane has been studied for relative spectral irradiance and spatial uniformity, both for the measurement beams from the LEDs, and the bias lights provided by the halogen lamp towers.

Figure 5 shows the measured spectra  $E_i(\lambda)$  of the measurement LEDs assembled. In the data analysis, only the relative spectra are needed but the spectra presented have been scaled to the levels in the measurement plane. The integrated

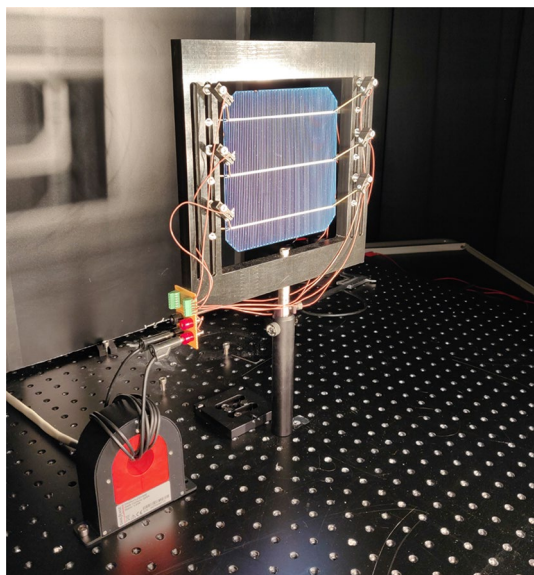


**Fig. 4** A holder for  $15 \times 15 \text{ cm}^2$  unifacial or bifacial solar cells. Cell current is read from the busbars using six brass contacts. The rear side of the holder contains similar arrangement for measuring the backside of bifacial cells. The cell has been short-circuited through the sensor of a zero-flux on the left

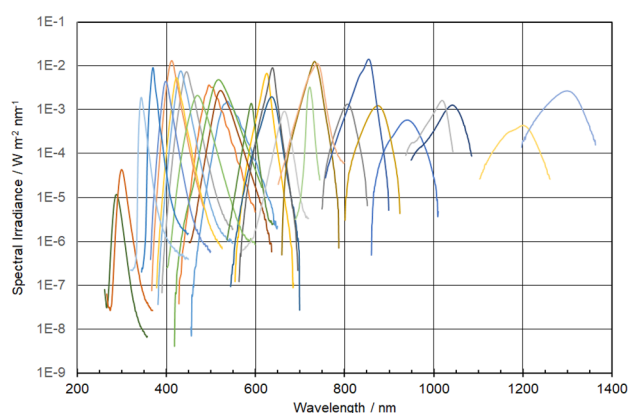


**Fig. 5** Spectra of the measurement LEDs

irradiance of the LED spectra vary within  $9\text{--}440 \text{ mW m}^{-2}$  depending on the LED. The LEDs cover a wavelength range of 290–1300 nm. The LEDs are not equally spaced, which in intercomparisons and interpretations of results is taken into account by interpolation.

The spectra were measured with an InstrumentSystems Spectro 320D scanning spectroradiometer, and an Ocean Optics USB4000 spectrograph. Bandwidths used varied within 1–10 nm. Measurements with the USB4000 have been fully automated with LabView, which provides a quick check for all LEDs within the visible region.

Figure 6 presents an example of the spatial uniformity measurements. Spatial uniformities of the light beams of all LEDs were measured using automated Newport linear translators over an area of  $15 \times 15 \text{ cm}^2$  with a step size of 1.5 cm, and over a smaller region of  $2 \times 2 \text{ cm}^2$  with a step size of 1 cm. The data were normalized to the values in the center of the measurement area, and used to calculate averages, standard deviations, and standard deviations of the mean for all LEDs, for the two measurement areas. The average of the spatial uniformity is used for correcting the measurement results, because in cell measurements, the reference detector measures the intensity over a small area in the middle only, whereas the cell sees a larger area. Standard deviation of the mean gives the uncertainty of the area correction, and the standard deviation can be used to estimate uncertainties due to alignment issues. In the measurements, a photometer with an entrance aperture of 10 mm in diameter for visible LEDs, a GaP photodiode with an entrance aperture of  $3 \times 3 \text{ mm}^2$  for UV, and an InGaAs photodiode with an entrance aperture of 5 mm in diameter for near-IR LEDs were scanned across the sample plane. For the 543-nm LED in Fig. 6, the average is  $-0.3\%$  over the full area of  $15 \times 15 \text{ cm}^2$  and  $0.0\%$  over the area of  $2 \times 2 \text{ cm}^2$ . The corresponding standard deviations are 0.4% and 0.1%. On the average, for all the 30 LEDs, the spatial uniformity correction was 1.8%, the maximum being 11%.

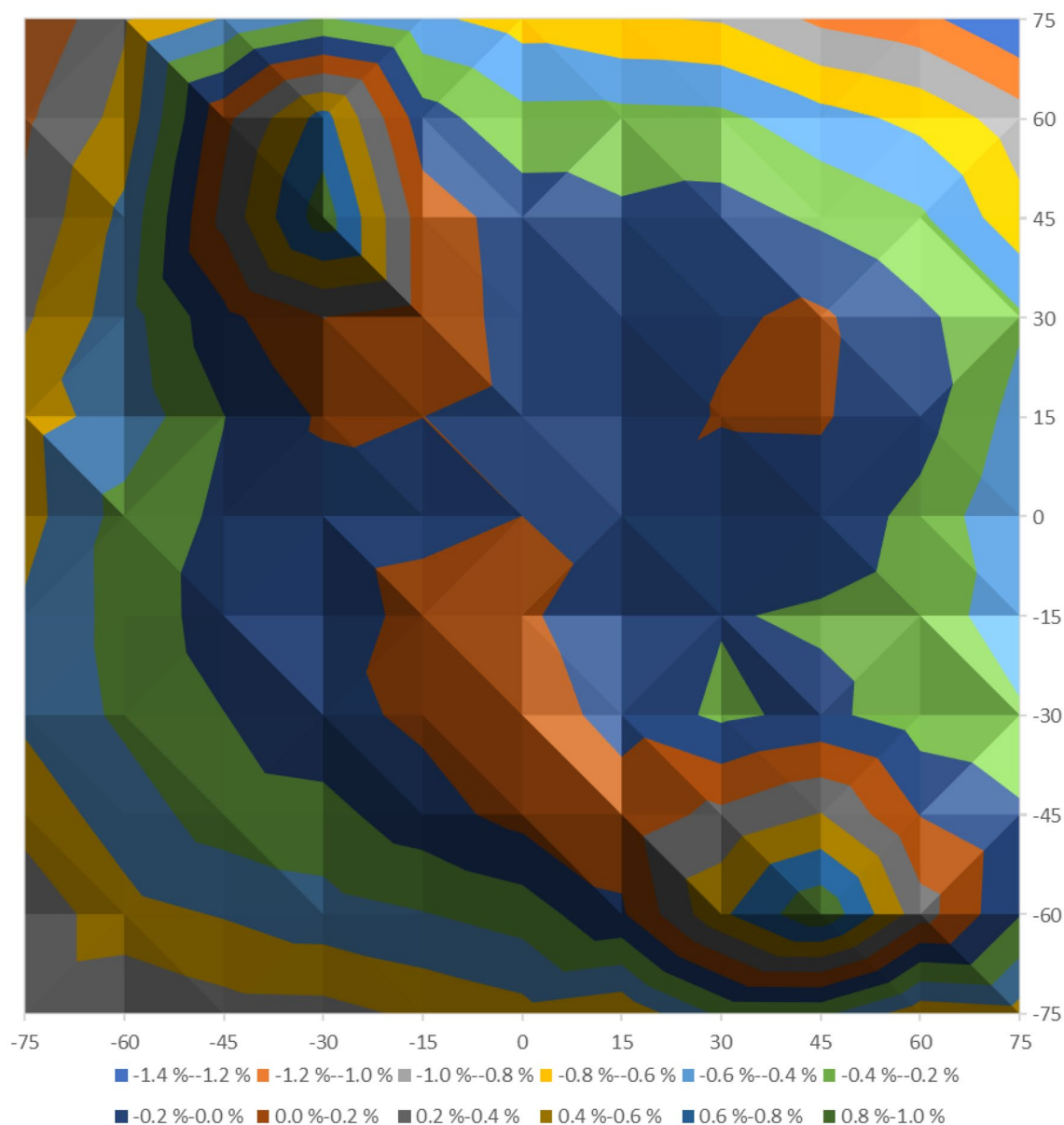


**Fig. 6** Spatial uniformity of the spectral irradiance produced by the 543 nm LED on the sample plane, calculated as deviation from the central value. The spacing between the different colors is 0.2%. The

spatial uniformities were measured over an area of  $15 \times 15 \text{ cm}^2$ . The units on the axes are mm (color figure online)

Temporal stability of the LEDs is an issue. This was studied by measuring their irradiances in the beginning of the measurements, and after about 3 weeks at the end of measurements. In between, the measurements had been running quite extensively. The average of the intensity changes of all 30 LEDs was 0.37%. Aging was most notable in the two IR LEDs at the wavelengths of 1187 and 1288 nm. Their intensities had dropped by 1.7%. With the other LEDs, changes were much smaller, on the average 0.28%.

Figure 7 shows the spectral irradiance and Fig. 8 the spatial uniformity of the spectral irradiance at the sample plane

produced by the four front side bias light towers. All  $4 \times 7$  lamps were on. The spectral irradiance is  $997.83 \text{ W/m}^2$  over the spectral range of 250–2150 nm which is close to the value of  $992.9 \text{ W/m}^2$  that the tabulated values for AM1.5 at  $1000 \text{ W/m}^2$  would produce across the same wavelength range. In the UV region, the halogen lamp source cannot fully replicate the spectrum. In the visible and near-IR regions, where solar cells have the highest responsivities, the agreement is better.

For the spatial uniformity of bias lights, the standard deviation is 8.9% over the full area of  $15 \times 15 \text{ cm}^2$ . The maximum value is 0.8%, the minimum is  $-37.3\%$ , and the

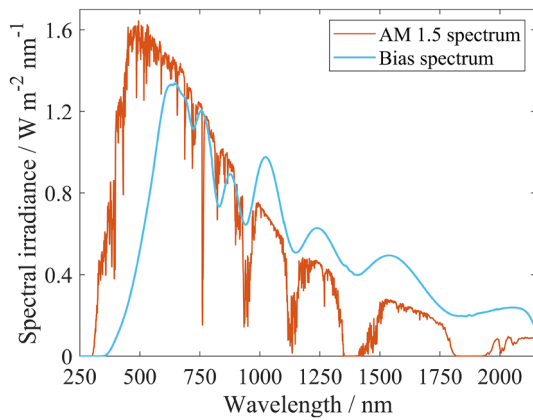


**Fig. 7** Spectral irradiance produced by the four front bias light towers on the sample plane and the AM1.5 (G) spectrum for comparison

average is  $-13.3\%$ . The maximum is located slightly below the center, and the radiation gradually drops towards the edges. The average indicates that the intensity across the cell is this much lower than the measured intensity in the center, which can be taken into account when measuring large cells. For the smaller  $2 \times 2 \text{ cm}^2$  area, the average of the spatial uniformity is  $+0.5\%$  and the standard deviation is  $0.9\%$ .

## 4 Data analysis

For characterization of a solar cell against the reference detectors, measurements are carried out as follows. First, the trap detector serving as reference with spectral responsivity  $R_{\text{trap}}(\lambda)$  [ $\text{A W}^{-1}$ ], is placed so that its precision aperture with area  $A_{\text{trap}}$  is in the sample plane. Measurements with all 30 LEDs with relative spectral irradiances  $E_i(\lambda)$  are carried out. A measurement with the LED unlit is carried out before each measurement to derive dark signals that are subtracted to derive photocurrents  $I_{\text{trap},i}$ . Next, the solar cell whose spectral responsivity  $S_{\text{cell}}(\lambda)$  [ $\text{A W}^{-1} \text{m}^2$ ] is to be derived, is placed so that its active surface with area  $A_{\text{cell}}$  is in the sample plane. Measurements with all 30 LEDs are carried out to derive photocurrents  $I_{\text{cell},i}$  taking into account dark signals similar to trap measurements.

The measurements with a reference detector and the solar cell at each LED give one responsivity  $S_{\text{cell}}(\lambda_{\text{eff},i})$  at the effective wavelength

$$\lambda_{\text{eff},i} = \frac{\int E_i(\lambda) \lambda d\lambda}{\int E_i(\lambda) d\lambda} \quad (1)$$

of the measurement. These are the wavelengths that will have most effect on the signals produced. The LEDs are rather broadband, which needs to be taken into account in the analysis [8]. To do this, a recursive analysis method is used. We first make an initial guess for the spectral responsivity of

the solar cell being measured as  $S_{\text{cell}}(\lambda) = 1 \text{ A W}^{-1} \text{m}^2$ . The initial values are being used to calculate the currents that theoretically can be expected as

$$I_{\text{calc,trap},i} = A_{\text{trap}} \int_{\lambda} E_i(\lambda) R_{\text{trap}}(\lambda) d\lambda \quad (2)$$

for the silicon trap detector, and

$$I_{\text{calc,cell},i} = \int_{\lambda} E_i(\lambda) S_{\text{cell}}(\lambda) d\lambda \quad (3)$$

for the current produced by the solar cell. The spectral irradiances of the LEDs are only known relatively, so they are effectively adjusted using  $I_{\text{trap},i}$  and  $I_{\text{calc,trap},i}$ . First real values for the spectral responsivity of the cell at the effective wavelengths can now be calculated as

$$S'_{\text{cell}}(\lambda_{\text{eff},i}) = \frac{I_{\text{cell},i} I_{\text{calc,trap},i}}{I_{\text{calc,cell},i} I_{\text{trap},i}} S_{\text{cell}}(\lambda_{\text{eff},i}). \quad (4)$$

The first values are accurate in the regions where the relative spectral responsivities of the solar cell and the reference detector are similar. In case of the silicon trap detector, this applies to the visible region. However, in the UV and IR regions, where the responsivities are different, the spectral shape assumed for  $S_{\text{cell}}(\lambda_{\text{eff},i})$  affects the results. The results can be improved by interpolating the  $S'_{\text{cell}}(\lambda_{\text{eff},i})$  values, placing these interpolated values as  $S_{\text{cell}}(\lambda)$  in Eq. 3 and repeating the calculations to derive  $S''_{\text{cell}}(\lambda_{\text{eff},i})$ . The interpolation can be done with piecewise polynomials, one for UV region, one for visible, and one for IR regions. The iteration quite soon finds a solution where the values do not change anymore. If the relative shape of the solar cell responsivity is known, e.g. from earlier measurements, this responsivity can be used to speed up the analysis. The data analysis results in an interpolation function and accurate spectral responsivity values at the effective wavelengths of the LEDs. Based on the differences of the first calculation assuming flat responsivity from the final solution, we may conclude the uncertainty caused by this modeling to be smaller than  $0.1\%$  in the wavelength region  $400\text{--}940 \text{ nm}$ , smaller than  $0.5\%$  in the UV excluding the shortest wavelength, and smaller than  $2\%$  in the IR excluding the longest wavelength. The extreme values will have approximately double the uncertainty.

## 5 Validation and test measurements

### 5.1 Fraunhofer ISE reference cell

To validate the measurement setup, a reference cell calibrated by Fraunhofer ISE was measured [15] with all the

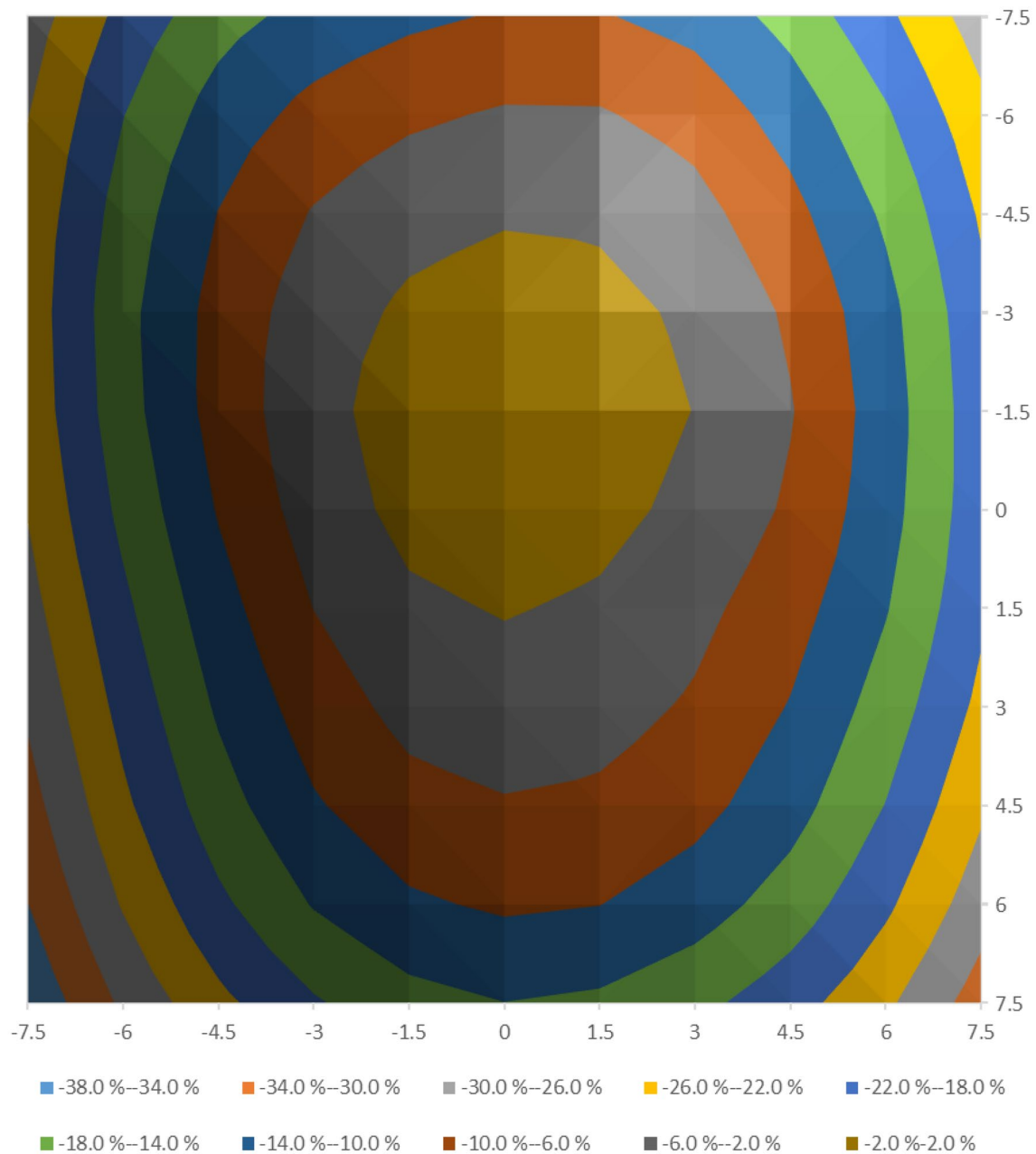


**Fig. 8** Spatial uniformity of the spectral irradiance produced by the four front bias light towers on the sample plane, calculated as deviation from the central value. The spacing between the different

colors is 4%. The spatial uniformity was measured over an area of  $15 \times 15 \text{ cm}^2$ . The units on the axes are mm (color figure online)

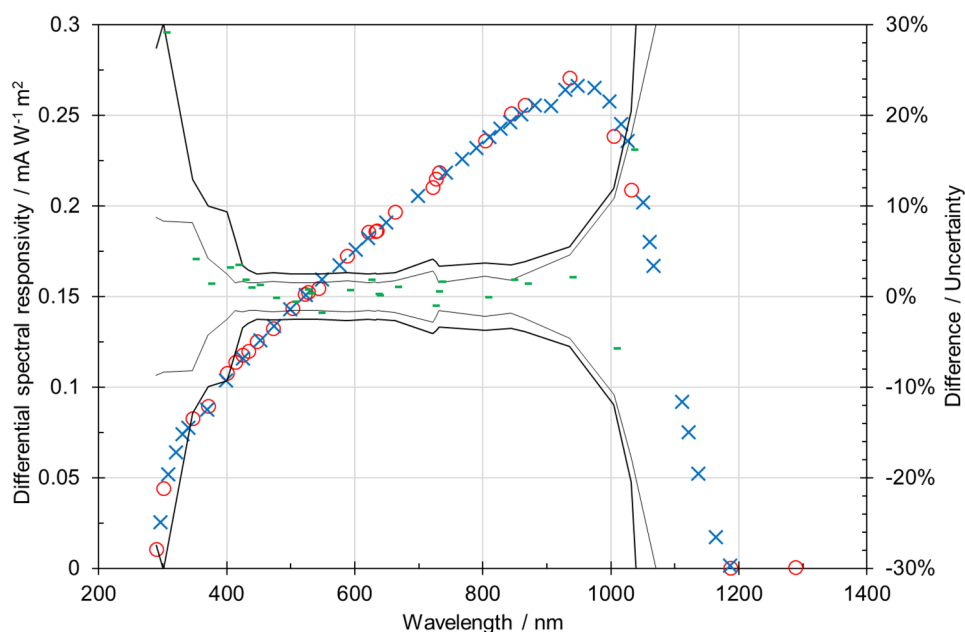
four towers of front bias lights on. The photocurrent produced by the bias light was 131 mA which is 88% of the nominal short circuit current.

Comparison of the responsivities to the values of Fraunhofer ISE is presented in Fig. 9. The results are in good agreement in the visible region. The deviations are smaller than 2% within the wavelength range 425–940 nm. The maximum deviations in the visible region are 2.7% at 401 nm, 3.5% at 413 nm and 1.8% at 844 nm wavelengths.

In the UV region, we measure systematically higher. At 346 nm wavelength, the deviation is 1.4%, at 301 nm it is 4.2%, and at 290 nm it is 29%. We conclude that these problems in the UV region originate from too low signal levels, although this is not fully supported by the estimated uncertainties. The lowest AC current measured was 3 nA, which in the presence of 131 mA bias signal requires a dynamic range of 153 dB. In the IR region the discrepancies are high as well, probably originating from the



**Fig. 9** Comparison measurement of a  $2 \times 2 \text{ cm}^2$  reference solar cell. Blue crosses denote the spectral responsivities of Fraunhofer ISE, red circles denote the results of Aalto (left vertical scale). Green dashes show the deviation of the Aalto values from the interpolated values of Fraunhofer ISE (right vertical scale). The thin lines represent the expanded measurement uncertainties of Aalto, thick lines indicate combined uncertainties of the comparison taking also into account the uncertainties of Fraunhofer ISE (right vertical scale) (color figure online)



calibration and the temperature sensitivity of the silicon trap detector used.

The expanded uncertainty of the obtained differential spectral responsivities over the visible region 400–730 nm is on the average 1.7% ( $k=2$ ). The main components included are the standard uncertainties of the alignment, distance and spatial correction (0.25–0.9%), gain of the lock-in amplifier (0.5%), short-term stability of the LED sources (0.03–0.9%), absolute spectral irradiance (0.11%), relative spectral irradiance (0.5%), data analysis (0.1%), and the resolution of the current measurement (0.01–0.06%). The standard deviation of the mean of the spatial uniformity of the measurement beam is of the order of 0.02–0.31% depending on the LED used over the solar cell area of  $2 \times 2 \text{ cm}^2$ . In the UV and IR regions, the non-uniformities are higher, up to 0.45%. Also, other uncertainties are higher. The expanded uncertainty of the reference values of Fraunhofer ISE is 2% over the visible region, extending the uncertainty of the comparison in the mid-visible region to 2.6%. All deviations are within the calculated uncertainties indicating that the estimated uncertainties are realistic.

Linearity of the cell was tested by varying the bias light level by switching off lights from the light towers and measuring the responsivity at the wavelength of 503 nm. The results indicate that the cell linearity is better than 0.01% within photocurrent range 0.12 mA–131 mA.

## 5.2 Large bifacial solar cell

The  $15 \times 15 \text{ cm}^2$  bifacial solar cell was studied at various lighting levels including  $1000 \text{ W/m}^2$  on the front side,  $1000 \text{ W/m}^2$  on the front side and  $300 \text{ W/m}^2$  on the rear side,

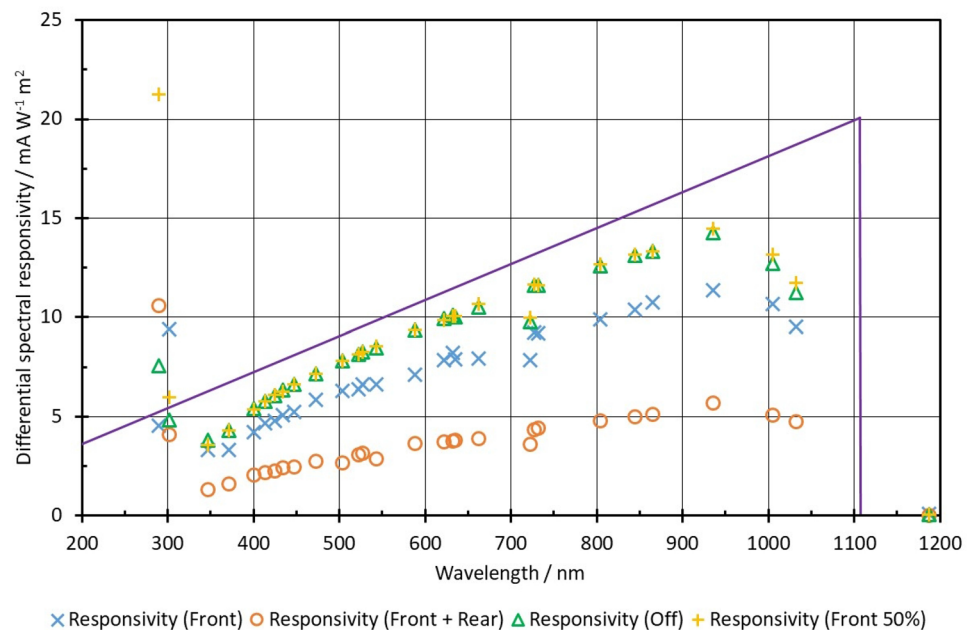
$500 \text{ W/m}^2$  on the front side, and bias lighting off. The results are depicted in Fig. 10.

The results with bias off and 50% bias on the front side are very close to each other. The responsivities measured with bias in the near IR, 900–1050 nm, are 2–4% higher than the responsivities without bias. We conclude this to be because of increasing temperature of the bifacial cell. The effect can be further seen in the shapes of the spectral responsivities measured at higher biases. The reason for the reduced responsivity at 722 nm wavelength is unknown.

Full bias lighting of  $1000 \text{ W/m}^2$  on the front surface introduces  $-20\%$  drop in the responsivity of the panel. Adding  $300 \text{ W/m}^2$  on the rear side increases this decrease to  $-60\%$ . This appears to be a property of the burden voltage of the cell that increases too high. Although the zero-flux does not load the circuit being measured, the wire used to short circuit the solar cell has a resistance of  $15 \text{ m}\Omega$ . With a short circuit current of 7.1 A corresponding to the four front light towers on, the voltage drop is 0.11 V which is too high considering that the open circuit voltage of the cell is only 0.565 V. With the added rear lights, the current increased to 8.4 A, and with 50% of the front lights on, it reduced to 3.5 A. This measurement demonstrates that in practice, it is impossible to measure such large cells without an active control of the cell current in the standard operating conditions with an irradiance of  $1000 \text{ W/m}^2$ . However, the zero-flux could be an excellent method of measuring currents of solar panels that have higher open circuit voltages. The zero-flux used is capable of handling currents up to 300 A with an uncertainty of 22 ppm.

Results of the biased cell also demonstrate nonlinearity induced by the varying levels of LED intensities. The biased curves contain fine structure that is not present in the

**Fig. 10** Differential spectral responsivity for the  $15 \times 15 \text{ cm}^2$  bifacial solar cell. Bias light conditions ranging from all lights off to full lighting on both sides (100% front + 30% rear) are indicated in the figure legend. The solid purple line represents the ideal responsivity assuming 100% quantum efficiency



measurements in the linear region. Results in the UV region are too large due to the loss of measurement signal in the zero-flux, and due to too large signal dynamics of 130 dB.

## 6 Conclusions

We have developed a setup for measuring differential spectral responsivities of solar cells in bias light conditions. The setup uses 30 high-brightness LEDs for generating a quasi-monochromatic light source covering the wavelength range of 290–1300 nm. Halogen lamps are used to generate bias-lighting conditions up to  $1000 \text{ W/m}^2$ , with spectral distribution close to AM1.5 in visible and near IR, but deviating in the UV. The setup has been fully characterized for spectral irradiances and spatial uniformities of all light sources. A validation carried out using a reference cell of  $2 \times 2 \text{ cm}^2$  area demonstrated deviations smaller than 2% over the wavelength range of 425–940 nm, with an expanded uncertainty of 2.6%. The setup was further tested in measurements of a bifacial cell. Measurement was successful but it appeared that the  $15 \text{ m}\Omega$  resistance of the wire used to short circuit the cell was too high causing nonlinearity with the 7 A current produced when using all front light towers. The result indicates that active control of the cell voltage is required at high intensity levels of  $1000 \text{ W/m}^2$ . At the reduced intensity causing 3.5 A bias current, the cell still remained in its linear region.

**Acknowledgements** Open access funding provided by Aalto University. This work has received funding from project 16ENG02 PV-Enerate of the EMPIR programme co-financed by the Participating States and from the European Union's Horizon 2020 research and innovation programme.

**Open Access** This article is licensed under a Creative Commons Attribution 4.0 International License, which permits use, sharing, adaptation, distribution and reproduction in any medium or format, as long as you give appropriate credit to the original author(s) and the source, provide a link to the Creative Commons licence, and indicate if changes were made. The images or other third party material in this article are included in the article's Creative Commons licence, unless indicated otherwise in a credit line to the material. If material is not included in the article's Creative Commons licence and your intended use is not permitted by statutory regulation or exceeds the permitted use, you will need to obtain permission directly from the copyright holder. To view a copy of this licence, visit <http://creativecommons.org/licenses/by/4.0/>.

## References

1. IEC 60904-8:2014: Photovoltaic Devices—Part 8: Measurement of Spectral Response of a Photovoltaic (PV) Device. The International Electrotechnical Commission IEC, Geneva (2014)
2. IEC 60904-3:2008: Photovoltaic Devices—Part 3: Measurement Principles for Terrestrial Photovoltaic (PV) Solar Devices with Reference Spectral Irradiance Data. The International Electrotechnical Commission IEC, Geneva (2008)
3. Metzendorf, J.: Calibration of solar cells 1: the differential spectral responsivity method. *Appl. Opt.* **26**, 1701–1708 (1987)
4. Zaid, G., Park, S.-N., Park, S., Lee, D.-H.: Differential spectral responsivity measurement of photovoltaic detectors with a light-emitting-diode-based integrating sphere source. *Appl. Opt.* **49**, 6772–6783 (2010)
5. Hamadani, B.H., Roller, J., Dougherty, B., Persaud, F., Yoon, H.W.: Absolute spectral responsivity measurements of solar cells by a hybrid optical technique. *Appl. Opt.* **52**, 5184–5193 (2013)
6. Hamadani, B.H., Roller, J., Shore, A.M., Dougherty, B., Yoon, H.W.: Large-area irradiance-mode spectral response measurements of solar cells by a light-emitting, diode-based integrating sphere source. *Appl. Opt.* **53**, 3565–3573 (2014)

7. Winter, S., Wittchen, T., Metzdorf, J.: Primary reference cell calibration at the PTB based on an improved DSR facility. Presented at the 16th European Photovoltaic Solar Energy Conference, 2000, Glasgow
8. Tureka, M., Sporledera, K., Luka, T.: Spectral characterization of solar cells and modules using LED-based solarsimulators. *Sol. Energy Mater. Sol. Cells* **194**, 142–147 (2019)
9. Hamadani, B.H., Roller, J., Dougherty, B., Yoon, H.W.: Versatile light-emitting-diode-based spectral response measurement system for photovoltaic device characterization. *Appl. Opt.* **51**, 4469–4476 (2012)
10. Krebs, F.C., Sylvester-Hvid, K.O., Jørgensen, M.: A self-calibrating led-based solar test platform. *Prog. Photovolt: Res. Appl.* **19**, 97–112 (2011)
11. Rauer, M., Guo, F., Hohl-Ebinger, J.: Accurate measurement of bifacial solar cells with single- and both-sided illumination. Presented at the 36th European PV Solar Energy Conference and Exhibition, 9–13 September 2019, Marseille, France
12. Hirvonen, J.-M., Poikonen, T., Vaskuri, A., Kärhä, P., Ikonen, E.: Spectrally adjustable quasi-monochromatic radiance source based on LEDs and its application for measuring spectral responsivity of a luminance meter. *Meas. Sci. Technol.* **24**, 115201 (2013)
13. Baumgartner, H., Vaskuri, A., Kärhä, P., Ikonen, E.: A temperature controller for high power light emitting diodes based on resistive heating and liquid cooling. *Appl. Therm. Eng.* **71**, 317–323 (2014)
14. Kärhä, P., Toivanen, P., Haapalinna, A., Manoochehri, F., Ikonen, E.: Filter radiometry based on direct utilization of trap detectors. *Metrologia* **35**, 255–259 (1998)
15. Fraunhofer ISE CalLab PV Cells, Heidenhofstr.2, 79110 Freiburg, Germany. German Accredited Calibration Laboratory No. D-K-11140-01-00

**Publisher's Note** Springer Nature remains neutral with regard to jurisdictional claims in published maps and institutional affiliations.